

# Out-of-autoclave manufacturing of GLARE panels using resistance heating

Bernhard Müller, Genevieve Palardy, Sofia Teixeira De Freitas, Jos Sinke

*Delft University of Technology, Klyverweg 1, 2629 HS Delft*

---

## Abstract

Autoclave manufacturing of fibre metal laminates, such as GLARE, is an expensive process. Therefore, there is an increasing interest to find cost-effective out-of-autoclave manufacturing processes without diminishing the laminate quality. The aim of this study is to evaluate the quality of fibre metal laminate panels adhesively bonded and cured using resistance heating. Three manufacturing processes are compared for different layups with an embedded steel mesh at the mid-plane: autoclave curing, resistance bonding of two (autoclave-cured) panels, and complete out-of-autoclave resistance curing of panels. Interlaminar shear strength tests and optical microscopy analysis showed that resistance bonding is a promising technique, leading to results comparable to autoclave curing. Resistance curing led to an interlaminar shear strength decrease of 30-60%. A study of the correlation between degree of cure and distance from the mesh revealed the potential of resistance bonding to be used for flexible embedded mesh geometries and on-site repairs.

*Keywords:* Out-of-autoclave, Resistance heating, Fibre metal laminates (FMLs)

---

## 1. Introduction

Fibre metal laminates (FMLs) were developed to reduce the weight and increase the damage tolerance of metallic lightweight structures [1]. They are composed of alternating metallic sheets and fibre-reinforced epoxy layers [2].

---

<sup>1</sup>s.teixeiradefreitas@tudelft.nl

5 An FML currently used in the aircraft industry is glass laminate aluminium  
6 reinforced epoxy, most commonly referred to as GLARE [3, 4].

7 The main advantage of GLARE, compared to monolithic aluminium struc-  
8 tures, is its lower fatigue crack growth rate [5, 6]. In addition, what sets it  
9 apart from pure glass fibre laminates is its advanced impact properties [7],  
10 higher moisture- and UV-resistance [8], favourable bearing strength and light-  
11 ning resistance [2, 4, 9].

12 Currently, autoclave manufacturing is the only process that delivers high  
13 quality GLARE panels needed for aerospace applications. However, it is an  
14 expensive process, especially when it comes to large parts [10, 11, 12]. More-  
15 over, a second autoclave cycle is often needed to reinforce GLARE panels, for  
16 instance in the vicinity of door holes in fuselage panels, in which GLARE dou-  
17 blers or thin aluminium sheets are bonded to the original GLARE fuselage  
18 skin [13]. Apart from the manufacturing costs, previous research has shown  
19 that exposing cured GLARE panels to elevated temperatures and thermo-  
20 cyclic loads, for example in a second autoclave cycle, can have a detrimental  
21 effect on the material properties [14, 15, 16, 17, 18, 19, 20].

22 Research findings have been reported on out-of-autoclave techniques that  
23 can allow localized curing and/or bonding of thermosets. Their common goal  
24 is to reduce production costs and focus heating on specific areas. Microwave  
25 radiation [21, 22, 23] and induction heating [24, 25, 26] have been investi-  
26 gated to cure or adhesively bond glass and carbon fibre reinforced thermoset  
27 composites. The resulting material properties were similar to those obtained  
28 with traditional manufacturing techniques, **but in some cases, the presence**  
29 **of defects, such as the amount of voids, increased and reached content values**  
30 **up to 20% due to the lower pressure applied during curing.**

31 Another potential localized out-of-autoclave manufacturing technique is  
32 resistance heating through the use of a metal mesh embedded at the bond-  
33 line or in the laminates. This method has been employed extensively to weld  
34 thermoplastic composite parts [27, 28, 29, 30, 31]. Those studies demon-  
35 strated the potential of resistance heating for joining composites and showed  
36 the effect of input parameters, materials and heater mesh on the quality of  
37 joints. The same concept has also been investigated to cure thermoset adhe-  
38 sives, resulting in high strength joints with potentially lower manufacturing  
39 costs [32, 33, 34]. An important aspect that has been investigated is the iden-  
40 tification of processing windows based on input parameters, such as heating  
41 elements configuration, to accelerate the curing process with resistance heat-  
42 ing [35, 36].

Using the concept of resistance heating to replace the autoclave curing process of GLARE, or to eliminate a second curing cycle when reinforcing GLARE panels, could lead to significant cost reductions. Autoclave manufacturing could be partly replaced by a less expensive, yet more adaptable equipment, consisting mainly of a vacuum bag and a power supply. This high flexibility brings new design opportunities for manufacturing innovative parts, as well as for repair applications. For instance, the location, position and shape of repair patches would be less restricted and on-site repairs using GLARE patches could be made possible. The shape of the resistance heater elements can be customizable and the temperature is generated only where it is required. The main concern is how the heating elements (or mesh) would affect the quality of the final laminate and how a uniform heating distribution can be guaranteed.

Therefore, the aim of this study is to evaluate the quality of FMLs adhesively bonded or cured using resistance heating. Three different manufacturing processes are compared: 1) autoclave curing of GLARE panels, 2) resistance bonding of two autoclave-cured GLARE panels, and 3) resistance curing of full GLARE panels (complete out-of-autoclave manufacturing). In order to assess the effect of the different manufacturing techniques, a detailed examination of the GLARE panels was carried out based on interlaminar shear strength (ILSS) tests and optical microscopy of the cross-sections and fracture modes.

## 2. Materials

Two types of GLARE laminates were used in this study: GLARE 3-4/3-0.3 and GLARE 5-4/3-0.3. Both laminates consist of four 0.3 mm thick 2024-T3 aluminium layers, bonded together with glass fibre prepregs S2-glass/FM94. The difference between GLARE 3 and GLARE 5 laminates lies in the layup sequence of the prepregs. In GLARE 3, each glass prepreg laminate between the aluminium plates is made of uni-directional (UD) plies with a layup of  $[0/90]$ . In GLARE 5, the layup is  $[0/90/90/0]$ . The complete layups of GLARE 3-4/3-0.3 and GLARE 5-4/3-0.3 are therefore  $[Al/0/90/Al/0/90/Al/90/0/Al]$  and  $[Al/0/90/90/0/Al]_{2s}$ , respectively.

Prior to bonding, the aluminium surfaces were pre-treated with chromic acid anodizing and primed with BR 127 (Cytec Engineered Materials, Tempe, Arizona, USA).

78 The specifications of the stainless steel heater mesh used in this study are  
79 listed in Table 1. It has a thickness of 0.8 mm and  $200 \times 200$  mesh per linear inch  
80 (25.4 mm).

Parameter	Dimension	Unit
Mesh per linear inch	$200 \times 200$	inch
Thickness	0.8	mm
Wire diameter	0.041	mm
Width of opening	0.089	mm
Open area	46	%
Material	AISI 304L	-

Table 1: Steel heater mesh specifications [37]

### 81 **3. GLARE panels manufacturing**

#### 82 *3.1. Manufacturing methods*

##### 83 *3.1.1. Reference method: autoclave curing*

84 The standard autoclave cycle for GLARE panels manufacturing is shown  
85 in Figure 1. The panels are cured at a temperature ( $T$ ) of  $120^\circ\text{C}$  for one  
86 hour, with heating and cooling rates of  $2^\circ\text{C}/\text{min}$ . The autoclave ( $P$ ) and  
87 vacuum bag ( $V$ ) pressures are maintained at 6 bar and 1 bar, respectively.  
88 In order to evaluate the effect of the steel mesh on the quality of the pan-  
89 els, independently of the manufacturing process, the autoclave was used to  
90 manufacture panels with and without a mesh, as schematically illustrated in  
91 Figures 2 (a) and (b).

##### 92 *3.1.2. Resistance bonding and curing*

93 The work presented in this paper distinguishes between resistance bond-  
94 ing (RB) and resistance curing (RC) of GLARE panels. In the case of the  
95 resistance bonding method, firstly, two separate GLARE panels are cured in  
96 the autoclave. Secondly, the two panels are brought together with an adhe-  
97 sive layer or glass prepreg layer in between. This layer is subsequently cured  
98 using resistance heating (out-of-autoclave secondary bonding), as shown in  
99 Figure 2 (c). In the case of resistance curing, all prepreg layers through the  
100 thickness are cured out-of-autoclave using resistance heating, as shown in  
101 Figure 2 (d).



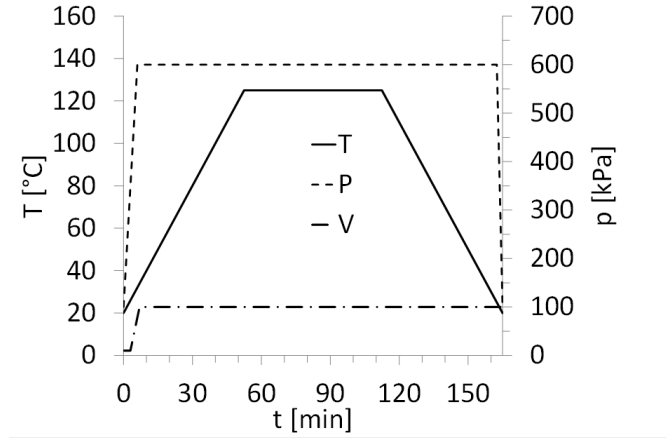


Figure 1: Standard manufacturing conditions for GLARE panels during the cure cycle: Temperature ( $T$ ), pressure in the vacuum bag ( $V$ ) and pressure in the autoclave ( $P$ ).

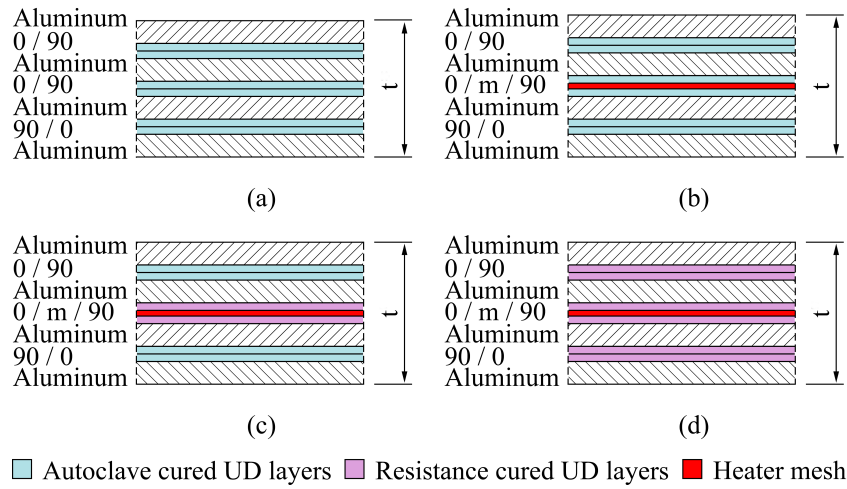


Figure 2: Overview of the investigated manufacturing techniques by means of a GLARE 3-4/3-0.3 layup: Fully autoclave cured (a) without and (b) with mesh, (c) resistance bonded and (d) fully resistance cured.

During both techniques, a voltage is applied to the metal mesh, which heats up due to its electrical resistance. By following the temperature set points given in the standard autoclave cycle (see Figure 1), it is possible to cure the thermoset layers close to the mesh. Therefore, for both methods, heat is generated from inside the panel, while in autoclave manufacturing, it comes from outside. Another difference compared to autoclave curing is the lower pressure, solely applied with a vacuum bag during the process.

The presence of the epoxy layers ensures electrical isolation between the heater mesh and the aluminium layers. In addition to this, the protective liner which is applied to each single aluminium layer has a very low electrical conductivity. Consequently, the chance of short circuits are reduced during manufacturing.

Figure 3 shows the setup used for resistance bonding and curing of GLARE panels. The main components are (1) the panels, (2) a vacuum bag with a valve, (3) an electrical in- and output, (4) a power supply, (5) four thermocouples and (6) thermometers. Two panels with the same layup were cured simultaneously to reduce manufacturing time and to investigate the possible differences in the process.

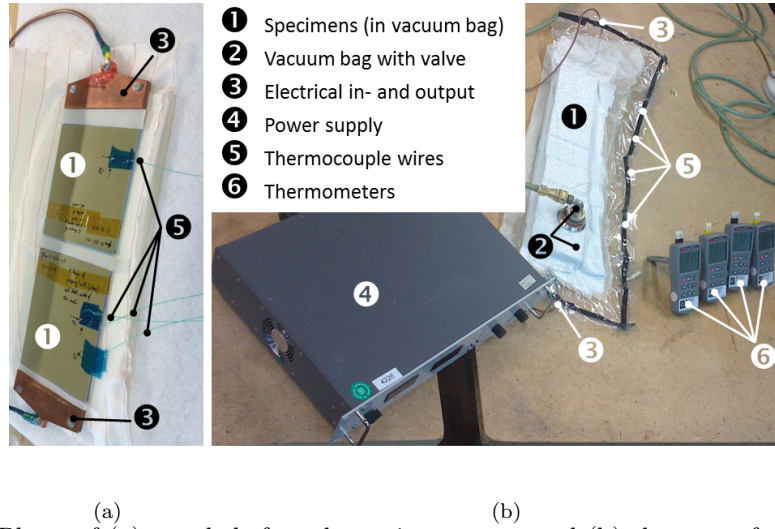


Figure 3: Photo of (a) panels before the curing process and (b) the setup for the out-of-autoclave bonding/curing of GLARE panels.

The direct voltage (DC) was provided by the power supply and controlled manually in order to follow the temperature set point shown in Figure 1. Three millimeter-thick copper clamps were used for the electrical in- and

123 output to ensure equal distribution of the current. The vacuum bag was  
124 used to generate a pressure of one bar. Thermocouples TC1 to TC3 were  
125 embedded in one panel and TC4, in the other. It was assumed that tem-  
126 perature profiles would be similar in both panels and that therefore, one  
127 thermocouple would be sufficient to monitor the process in the second panel.

### 128 3.2. GLARE panels layups

129 Two types of GLARE panels were manufactured: (1) “Full surface mesh”-  
130 panels and (2) “Mesh stripe”-panels. In the first, the steel mesh area covers  
131 the complete surface area of the GLARE panel. For this type, panels were  
132 manufactured using the three different methods mentioned in Section 3.1. In  
133 the second one, two autoclave cured GLARE panels were bonded using only  
134 a mesh stripe, 12.5 mm wide, positioned at the center of the panels. The aim  
135 was to assess the surface area of the embedded mesh needed to guarantee a  
136 certain degree of cure.

#### 137 3.2.1. Full surface mesh

138 A “Full surface mesh” panel indicates that the embedded mesh covered  
139 the entire surface area. In total, eight GLARE 3-4/3-0.3 and eight GLARE 5-  
140 4/3-0.3 panels were manufactured according to the layups listed in Tables 2  
141 and 3, respectively. A total of four panels were manufactured with an em-  
142 bedded mesh for each technique: autoclave (A3, A4, A7 and A8), resistance  
143 bonding (RB1-RB4) and resistance curing (RC1-RC4). Additionally, four  
144 reference samples were cured in the autoclave without mesh (A1, A2, A5  
145 and A6) to investigate its effect on the mechanical performance and quality  
146 of the panels. To examine the influence of the glass fibres on the impreg-  
147 nation of the heater mesh, panels with pure epoxy layers adjacent to the  
148 mesh were manufactured for the GLARE 3 and GLARE 5 layups (A3, A7,  
149 RB1, RB3, RC1, RC3). Figure 4 depicts the geometry of the panels and  
150 the position of the thermocouples during manufacturing of GLARE 3 and  
151 GLARE 5.

#### 152 3.2.2. Mesh stripe

153 One “mesh stripe” panel was manufactured according to the following  
154 procedure: two GLARE 5 panels were first cured in the autoclave, then  
155 bonded using resistance heating with a 12.5 mm wide mesh stripe. Figure 5  
156 shows the panel and mesh stripe dimensions, as well as the positions of  
157 five thermocouples (TC I to TC V) positioned on the outside surface of the

Abbr.	Manufacturing method	Layup
A1	Autoclave	Al/0/90/Al/PE/PE/Al/90/0/Al
A2	Autoclave	Al/0/90/Al/0/90/Al/90/0/Al
A3	Autoclave	Al/0/90/Al/PE/m/PE/Al/90/0/Al
A4	Autoclave	Al/0/90/Al/0/m/90/Al/90/0/Al
RB1	Res. bonding	Al/0/90/Al/ <u>PE</u> /m/ <u>PE</u> /Al/90/0/Al
RB2	Res. bonding	Al/0/90/Al/ <u>0</u> /m/ <u>90</u> /Al/90/0/Al
RC1	Res. curing	Al/0/ <u>90</u> /Al/ <u>PE</u> /m/ <u>PE</u> /Al/ <u>90</u> / <u>0</u> /Al
RC2	Res. curing	Al/0/ <u>90</u> /Al/ <u>0</u> /m/ <u>90</u> /Al/ <u>90</u> / <u>0</u> /Al

Table 2: Layups for the GLARE 3-4/3-0.3 panels. Underlined layers indicate they were cured using resistance (res.) heating. (*PE* and *m* are pure epoxy and mesh layers, respectively.)

Abbr.	Manufacturing method	Layup
A5	Autoclave	Al/0/90/90/0/Al/PE/PE/PE/PE/Al/0/90/90/0/Al
A6	Autoclave	Al/0/90/90/0/Al/0/90/90/0/Al/0/90/90/0/Al
A7	Autoclave	Al/0/90/90/0/Al/PE/PE/m/PE/PE/Al/0/90/90/0/Al
A8	Autoclave	Al/0/90/90/0/Al/0/90/m/90/0/Al/0/90/90/0/Al
RB3	Res. bonding	Al/0/90/90/0/Al/ <u>PE</u> / <u>PE</u> /m/ <u>PE</u> / <u>PE</u> /Al/0/90/90/0/Al
RB4	Res. bonding	Al/0/90/90/0/Al/0/ <u>90</u> /m/ <u>90</u> /0/Al/0/90/90/0/Al
RC3	Res. curing	Al/0/ <u>90</u> / <u>90</u> / <u>0</u> /Al/ <u>PE</u> / <u>PE</u> /m/ <u>PE</u> / <u>PE</u> /Al/0/ <u>90</u> / <u>90</u> / <u>0</u> /Al
RC4	Res. curing	Al/0/ <u>90</u> / <u>90</u> / <u>0</u> /Al/0/ <u>90</u> /m/ <u>90</u> /0/Al/0/ <u>90</u> / <u>90</u> / <u>0</u> /Al

Table 3: Layups for the GLARE 5-4/3-0.3 panels. Underlined layers indicate they were cured using resistance (res.) heating. (*PE* and *m* are pure epoxy and mesh layers, respectively.)

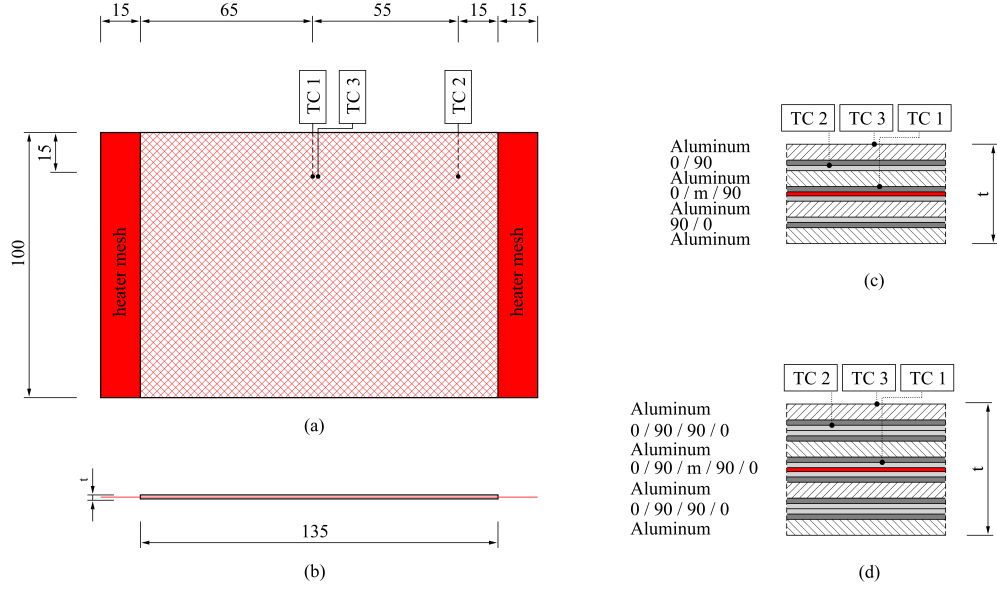


Figure 4: Dimensions of the full surface mesh panels: (a) Top view, (b) side view, details of (c) GLARE 3-4/3-0.3 and (d) GLARE 5-4/3-0.3 cross-sections with an integrated mesh ( $m$ ). Units are in millimetres.

GLARE panels. The layup of the panel is the same as the RB3 panel listed in Table 3.

The electrical current was controlled in such a way that the temperature at the surface of the panel above the mesh was between 120°C and 140°C - controlled by thermocouple I (TCI). This was done in order to increase the overall temperature in the vicinity of the heater mesh to insure a higher degree of cure could be reached.

### 3.3. Process parameters

#### 3.3.1. Full surface mesh

The temperature, electrical voltage and current curves were recorded during the out-of-autoclave manufacturing of GLARE panels using a full surface mesh. A representative example of the curves for resistance bonded GLARE 3 panels is shown in Figure 6 (a). The heating ramp rate and hold temperature of the four thermocouples, TC1 to TC4, closely follow the autoclave cycle. The cooling rate, however, slightly deviates from 2°C/min as no external cooling source was used. The electrical voltage was increased and adjusted

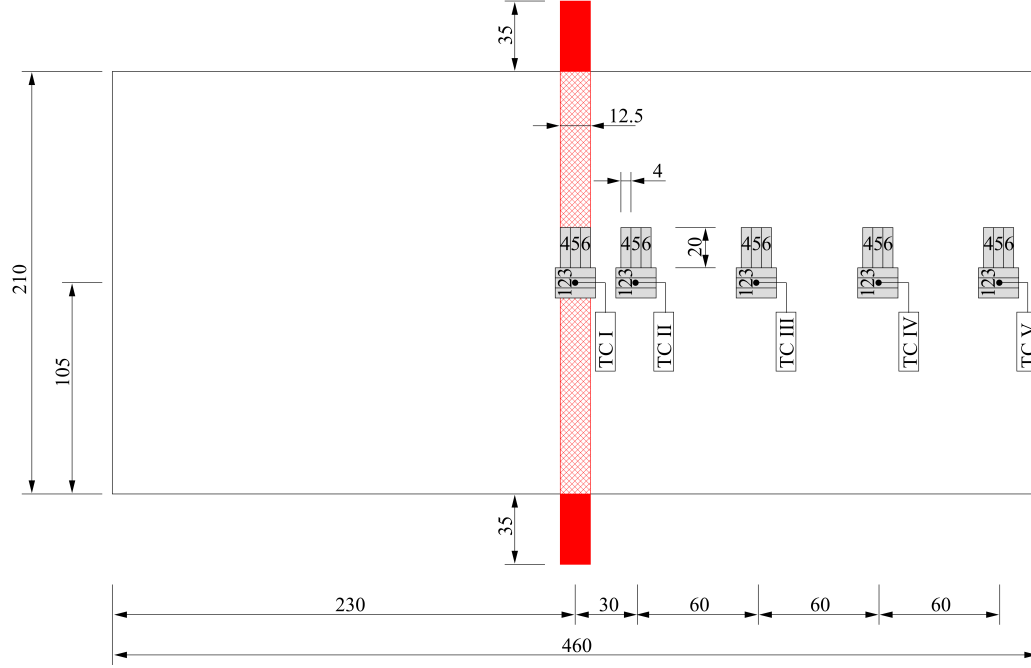


Figure 5: Dimensions of the mesh stripe panel, including the heater mesh (red), the positions of the thermocouples TC I to TC V and the ILSS specimens (grey). Units are in millimetres.

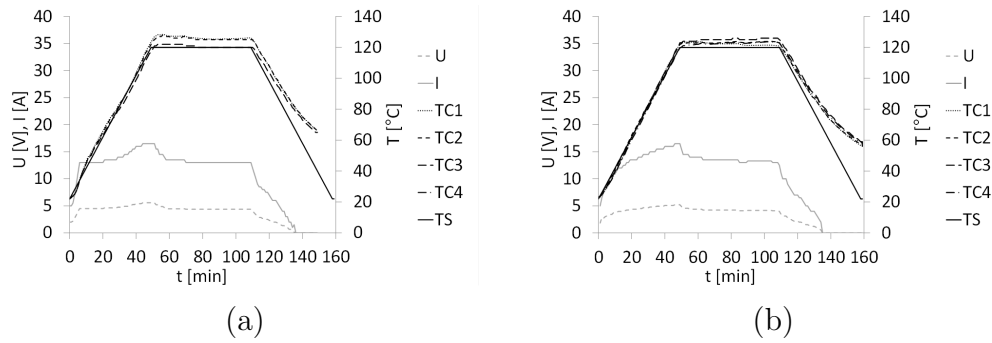


Figure 6: Temperature set point of autoclave cycle (TS), measured temperatures (TC1 to TC4), electrical voltage (U) and current (I) during (a) resistance bonding and (b) resistance curing of GLARE 3 panels with a full surface mesh.

174 during the cycle to keep the heating rate and hold temperature as constant  
 175 as possible.

176 Representative curves for resistance cured GLARE 3 panels are shown in  
 177 Figure 6 (b). They follow a pattern similar to those for resistance bonded  
 178 panels. Comparable curves were recorded during the manufacturing of the  
 179 GLARE 5 panels.

### 180 3.3.2. Mesh stripe

181 Figure 7 shows the temperature, electrical voltage and current curves  
 182 measured during resistance bonding of a GLARE 5 panel using a mesh stripe.  
 183 The temperature profiles at the locations near the mesh, TC I and TC II,  
 184 closely followed that of the autoclave cycle (TS). As expected, thermocouples  
 185 placed further away from the mesh, TC III to TC V, displayed a significant  
 186 drop in temperature, compared to TC II. The maximum temperature at  
 187 those locations reached values between 50°C and 80°C.

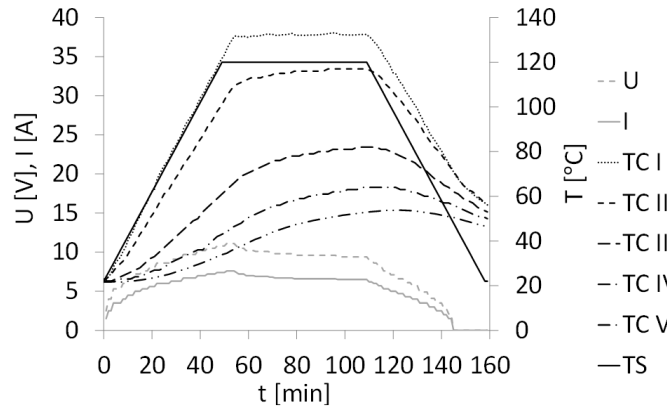


Figure 7: Temperature set point (TS), measured temperatures (TC I to TC V), electrical voltage (U) and current (I) during resistance bonding of the GLARE 5 panels with a mesh stripe.

## 188 4. Experimental methods

189 In order to evaluate the performance of the out-of-autoclave manufactur-  
 190 ing methods proposed in this work, interlaminar shear strength (ILSS) tests  
 191 were performed. It is expected to provide insights into manufacturing quality  
 192 and the effect of degree of cure on shear strength and adhesion of the epoxy  
 193 layers.

194 For each full surface mesh panels – listed in Tables 2 and 3 – six ILSS  
 195 specimens, 10 mm wide and 20 mm long, were cut from the GLARE panels.  
 196 Three specimens were tested with the length in the  $0^\circ$  direction and three  
 197 specimens in the  $90^\circ$  direction.

198 In the case of the mesh stripe panel, a total of six ILSS specimens in the  
 199  $0^\circ$  and  $90^\circ$  directions were tested for each thermocouple position in order  
 200 to investigate the correlation between the distance from the mesh and the  
 201 resulting effect on the ILSS values (see positions in Figure 5). The specimen  
 202 dimensions were 4 mm  $\times$  20 mm to focus more specifically on locations  
 203 where different degrees of cure were expected.

204 The ILSS tests were performed according to the ASTM D2344 standard  
 205 for short-beam strength of polymer matrix composite materials and their  
 206 laminates [38]. A schematic figure of the setup is given in Figure 8. The  
 207 loading span length-to-specimen thickness ratio was kept to 4.0 as recom-  
 208 mended by the ASTM standard. In both cases, all ILSS tests were conducted  
 209 on a 25 kN press with a test speed of 1 mm/min. During tests, the load-  
 210 displacement curves were recorded. After testing, the failure mode of the  
 211 ILSS specimens was examined with a high-resolution Keyence stereomicro-  
 212 scope. Furthermore, the manufacturing quality of the panels was assessed  
 213 through cross-sectional microscopy.

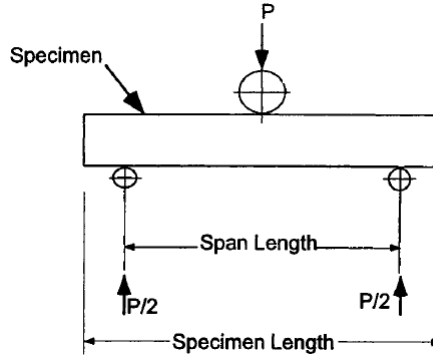


Figure 8: Schematic representation of the ILSS setup [38].



## 214 5. Experimental results

### 215 5.1. Full surface mesh panels

#### 216 5.1.1. Mechanical performance

217 Figure 9 shows representative force-displacement ( $F - \delta$ ) curves of the  
 218 ILSS tests for GLARE 3 samples manufactured by all three methods de-  
 219 scribed in Section 3.1 – for the complete layup of the panels please see Ta-  
 220 bles 2 and 3. The autoclave specimens manufactured without a mesh (A1)  
 221 displayed the steepest slope, followed by a sharp decrease in the load when  
 222 fracture occurred. The slope of the curves, proportional to the stiffness of the  
 223 specimens, slightly decreased when a mesh was placed at the interface (A3  
 224 and RB1). For A3 and RB1 layups, the curves followed a similar trend and  
 225 reached a maximum force close to A1, but at a higher displacement value.  
 226 The RC1 layup deviated from the other samples and presented a lower stiff-  
 ness and maximum load.

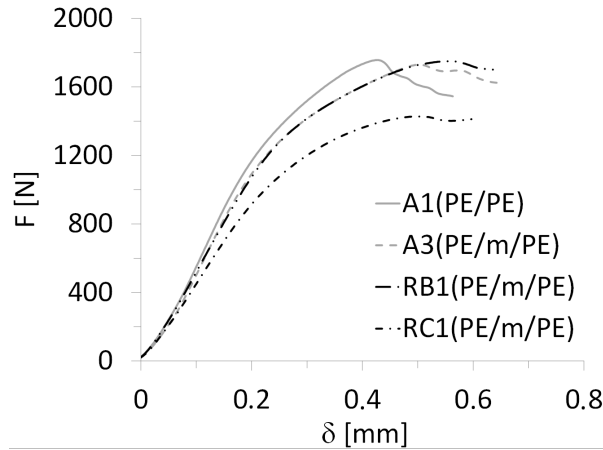


Figure 9: Typical force-displacement curves of ILSS tests on GLARE 3 specimens manufactured by autoclave, resistance bonding and resistance curing when using a full surface mesh.

227

228 Figure 10 (a) schematically depicts the main failure modes observed in  
 229 ILSS specimens for GLARE 3 panels. Intralaminar failure in the prepreg  
 230 layer, close to the aluminium layer (Figure 10 (b)) mainly occurred for  
 231 autoclave-cured samples without and with a mesh, A1 to A4 (Table 2),  
 232 as well as for resistance bonded specimens with pure epoxy layers at the  
 233 mesh (RB1). On the other hand, failure at the mesh interface (Figure 10 (c))

234 was only observed for resistance bonded panels when prepreg layers were  
 235 placed at the interface (RB2 layup). For resistance cured specimens (RC1  
 236 and RC2), fracture took place in the outer prepreg layers, as shown in Fig-  
 237 ure 10 (d). It is to be noted that similar failure modes were found for  
 238 GLARE 5 samples.

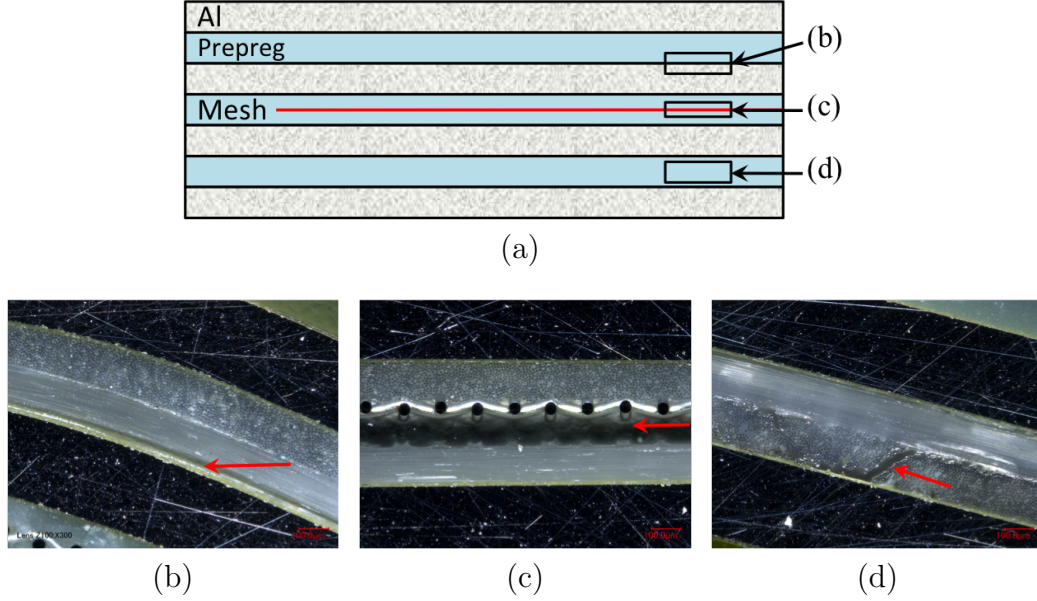


Figure 10: Typical failure modes: (a) Schematic GLARE cross-section with failure mode locations (red arrows) and representative cross-sectional microscopy images of (b) intralaminar failure in prepreg layer close to aluminium layer, (c) failure at the mesh interface, (d) intralaminar failure in the outer prepreg layers. Scale: 100  $\mu\text{m}$ .

239 The interlaminar shear strength was calculated based on the maximum  
 240 force measured in the force-displacement curves (Figure 9), as given by the  
 241 ASTM D2344 standard:

$$\tau_{ILSS} = \frac{0.75 F_{max}}{W L} \quad (1)$$

242 where  $F_{max}$  is the maximum load, and  $W$  and  $L$  are the width and length  
 243 of the specimen, respectively. Figure 11 and Table 4 summarize the ILSS  
 244 values for (a) GLARE 3 and (b) GLARE 5 specimens manufactured by au-  
 245 toclave, resistance bonding and resistance curing methods. The figure shows  
 246 the average values and the scatter range of the five ILSS tests conducted for  
 247 each configuration as listed in Tables 2 and 3.

For both GLARE 3 and GLARE 5 samples manufactured in the autoclave (A1 to A8), the heater mesh did not have a significant effect on the ILSS values, remaining within scatter range. Resistance bonded specimens (RB1 to RB4) displayed similar shear strength values to the autoclave panels, with the exception of RB2, which dropped to 47.7 MPa. This is consistent with the failure mode presented in Figure 10 (c), which is located at the mesh interface, likely due to poor resin impregnation because of the prepreg layers. When the panels were resistance cured, their average ILSS decreased by 27% to 31% for RC1 and RC2, and by 55% to 64% for RC3 and RC4, with comparison to the panels manufactured by autoclave with a mesh.

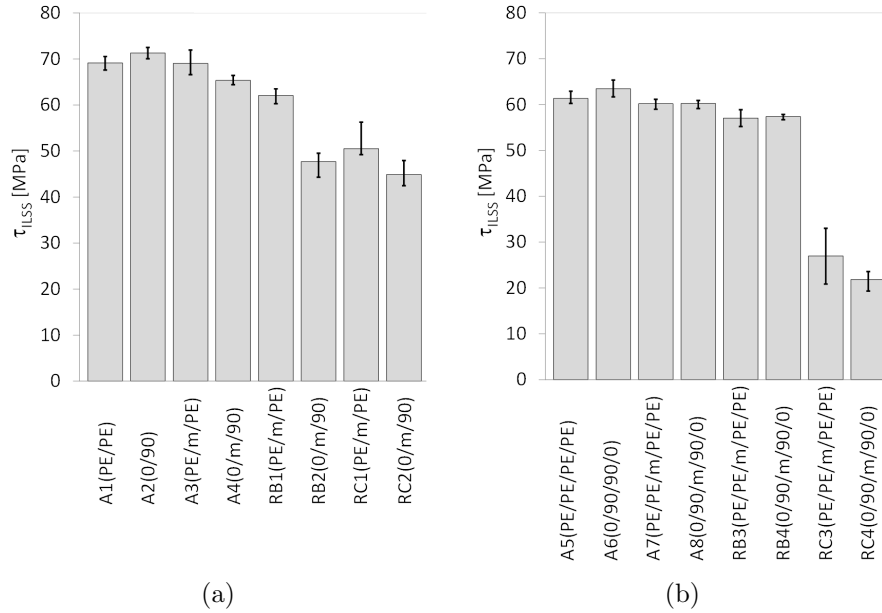


Figure 11: Average ILSS values for (a) GLARE 3 and (b) GLARE 5 specimens manufactured by autoclave, resistance bonding and resistance curing, according to the layups listed in Tables 2 and 3. The error bars show the scatter range with minimum and maximum ILSS values for each group of specimens.

### 5.1.2. Optical microscopy analysis

Cross-sections of the panels manufactured according to the methods and layups presented in Tables 2 and 3 were observed by optical microscopy to provide insight regarding the mechanical performance presented in Sec-

GL3	$\tau_{ILSS}$ [MPa]	GL5	$\tau_{ILSS}$ [MPa]
A1	69.2	A5	61.3
A2	71.3	A6	63.5
A3	69.1	A7	60.2
A4	65.3	A8	60.3
RB1	62.1	RB3	57.1
RB2	47.7	RB4	57.4
RC1	50.5	RC3	27.0
RC2	44.9	RC4	21.9

Table 4: Average ILSS values  $\tau_{ILSS}$  for the GLARE 3 (GL3) and GLARE 5 (GL5) specimens.

tion 5.1.1. Figure 12 shows representative images of GLARE 3 panels manufactured by all three methods and compares the heater mesh impregnation when using pure epoxy layers as the middle plies (A3, RB1 and RC1). Autoclave cured panels (Figure 12 (a)) exhibited the highest quality of mesh impregnation and the thinnest resin layer due to the higher pressure applied during manufacturing. It was observed that the presence of voids at the interface generally increased from resistance bonded (Figure 12 (b)) to resistance cured (Figure 12 (c)) panels. For the layups using prepreg layers only (A4, RB2 and RC2), the mesh impregnation significantly decreased compared to the use of pure epoxy layers, due to the lower resin content (Figure 13). Similarly to Figure 12, the presence of voids increased from autoclave (Figure 13 (a)), to resistance bonded (Figure 13 (b)), to resistance cured (Figure 13 (c)) panels. For the latter, a clear gap between the layers on both sides of the mesh was noticed.

The quality of the outer prepreg layers for GLARE 3 specimens manufactured by resistance bonding and curing is compared on Figures 14 (a) and (b), respectively. For resistance cured panels, several voids are present, especially at the aluminium-prepreg interface (Figure 14 (c)), possibly as a result of the lower pressure applied during out-of-autoclave manufacturing.

These observations can explain the failure modes witnessed in Figure 10. For resistance bonded specimens with prepreg layers (RB2), failure occurred at the mesh interface because of poor impregnation. The use of pure epoxy layers in the RB1 layup eliminated this weakness and therefore, this resulted into intralaminar failure, as seen in Figure 10 (b). For resistance cured

286 samples, fracture was noted in the outer prepreg layers, likely due to their  
 287 lower quality compared to the mesh impregnation. It is also possible that  
 288 residual stress concentrations developed during the curing process may have  
 289 contributed to crack initiation.

290 For GLARE 5 panels, the use of four pure resin layers at the mesh in-  
 291 terface (Figure 15) led to comparable impregnation to the GLARE 3 speci-  
 292 mens (Figure 12). It can be inferred that using only two pure epoxy layers  
 293 are sufficient for proper impregnation and quality.

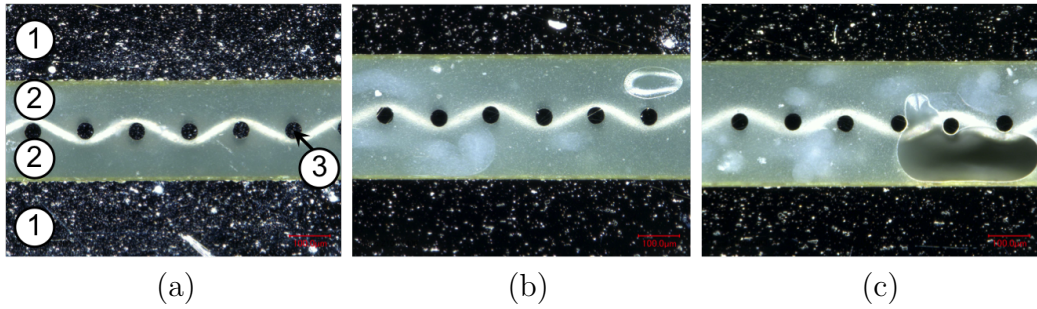


Figure 12: Cross-sectional microscopy images of GLARE 3 panels with embedded heater mesh between pure epoxy layers: (a) Autoclave manufacturing, (b) resistance bonding and (c) resistance curing. Legend: (1) aluminium layers, (2) pure epoxy layers and (3) heater mesh. Scale: 100  $\mu\text{m}$ .

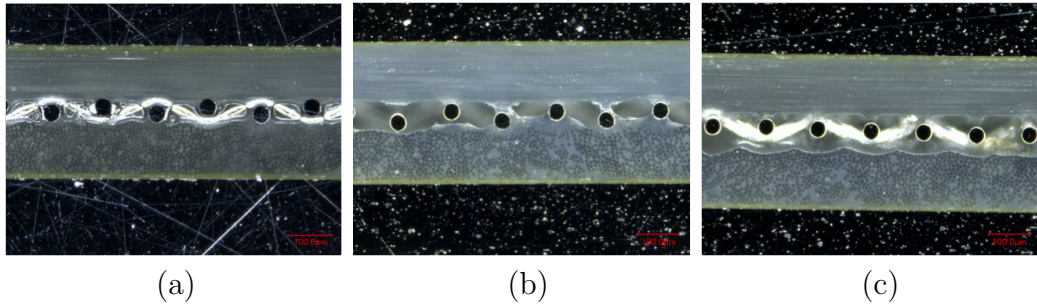


Figure 13: Cross-sectional microscopy images of GLARE 3 panels with embedded heater mesh between prepreg layers: (a) autoclave manufacturing, (b) resistance bonding and (c) resistance curing. Scale: 100  $\mu\text{m}$ .

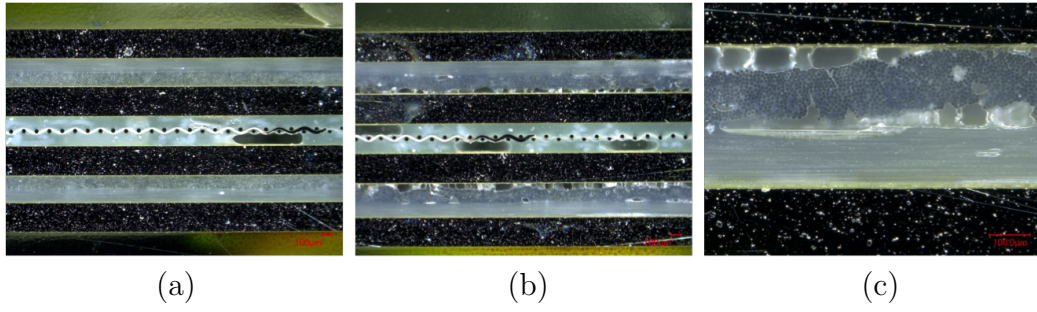


Figure 14: Cross-sectional microscopy images of GLARE 3 panels comparing the quality of the outer prepreg layers: (a) Resistance bonded panel, (b) resistance cured panel and (c) higher magnification image of bottom plies in (b). Scale: 100  $\mu\text{m}$ .

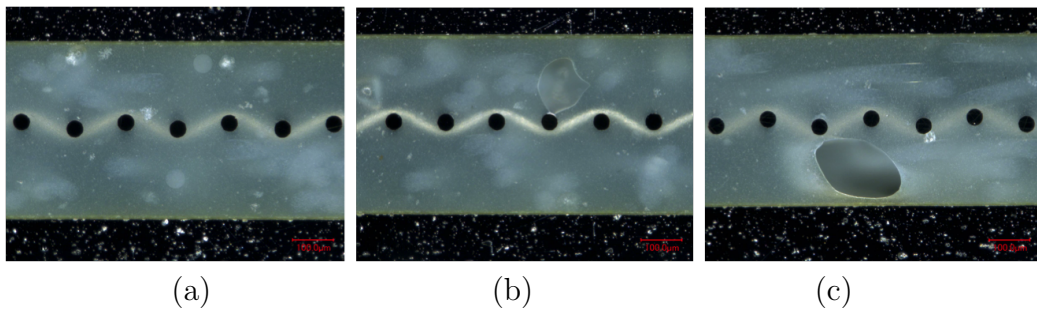


Figure 15: Cross-sectional microscopy images of GLARE 5 panels with embedded heater mesh with four pure resin layers: (a) Autoclave manufacturing, (b) resistance bonding and (c) resistance curing. Scale: 100  $\mu\text{m}$ .

## 294 5.2. Mesh stripe panel

### 295 5.2.1. Mechanical performance

296 Figure 16 shows representative  $F - \delta$  curves of the ILSS tests at the five  
 297 (thermocouple) positions (see Figure 5). The ILSS specimens for positions  
 298 TC I and TC II display the steepest  $F - \delta$  curve slopes, followed by a drop  
 299 in the load after failure. These positions also display the highest maximum  
 300 load when compared to the remaining positions (TC III, TC IV and TC V).

301 The  $F - \delta$  curves of the ILSS specimens from the positions TC III, TC IV  
 302 and TC V are significantly different. They approximate to a bi-linear be-  
 303 haviour – see Figure 16 for TC III-1. The initial slope is lower than for  
 304 positions TC I and TC II. After this initial slope, a significant plastic de-  
 305 formation plateau is followed before final failure. Although also present, the  
 306 change of slope and the plastic deformation in positions TC I and TC II is  
 307 almost insignificant when compared with positions TC III, TC IV and TC V.

308 As for the failure modes, positions TC I and TC II fail similarly as the  
 309 specimens for full surface mesh resistance bonding using pure epoxy (RB1  
 310 and RB3): intralaminar failure in the prepreg layer close to the aluminium  
 311 layer (Figure 10 (b)). This indicates a good adhesion on the curing process  
 312 of the resistance bonded layers. In fact, the  $F - \delta$  curves of positions TC I  
 313 and TC II are more comparable with the ones presented for the full surface  
 314 mesh specimens in Figure 9 than with the positions TC III to TC V.

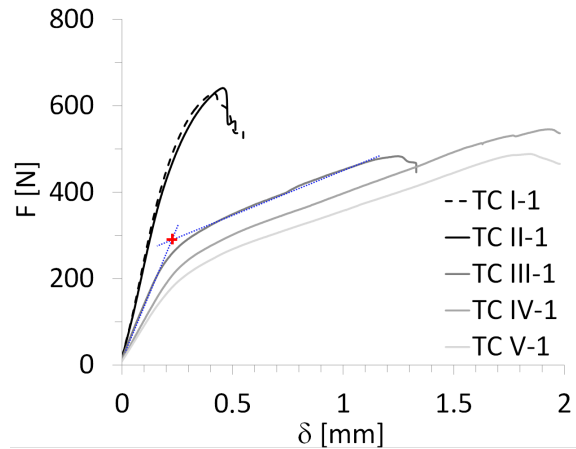


Figure 16: Representative force-displacement curves of ILSS tests on mesh stripe specimens – ‘+’ represents the bilinear intersection of the slopes.



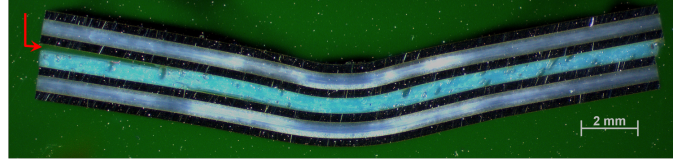


Figure 17: Cross-sectional microscopy image of a representative ILSS specimen at locations TC III, TC IV and TC V. The red arrow indicates the crack initiation.

315 The failure mechanism was significantly different for positions TC III,  
 316 TC IV and TC V. Figure 17 shows the typical failure mode of these speci-  
 317 mens. The final failure typically occurred at the interface between the pure  
 318 epoxy layers and the adjacent aluminium layers. This indicates a poor ad-  
 319 hesion quality during the curing process of those layers. In addition to this,  
 320 a significant permanent plastic deformation can be observed after failure.

321 This interface failure justifies the different  $F - \delta$  behaviour of the spec-  
 322 imens at positions TC III, TC IV and TC V when compared to TC I and  
 323 TC II. The (not-fully-cured) pure epoxy layer could not take significant longi-  
 324 tudinal shear stress and therefore could not guarantee the continuous strain  
 325 distribution through the laminate thickness. This discontinuity in strains  
 326 results in significantly higher normal stresses at the aluminium layers when  
 327 compared to the situation of continuous longitudinal strains through the lam-  
 328 inate thickness for the same load - as in the case of positions TC I and TC II.  
 329 Therefore, the aluminium layers yield at mid span at a much lower load level  
 330 for positions TC III, TC IV and TC V, as seen in Figure 16. The displace-  
 331 ment plateau shown at these curves corresponds probably to the aluminium  
 332 ductility after yield.

333 Figure 18 and Table 5 show the average ILSS values for the five positions,  
 334 both longitudinal direction (specimens 1 to 3) and transverse direction (spec-  
 335 imens 4 to 6). For positions TC I and TC II, the ILSS values were determined  
 336 using the maximum load value, as was the case for full surface mesh samples  
 337 (Section 5.1.1). For positions TC III, TC IV and TC V, the ILSS values were  
 338 determined using a bilinear intersection - marked as ‘+’ in Figure 16. There  
 339 are two main reasons to use the intersection values for the latter positions.  
 340 Firstly, the  $F - \delta$  curve and the failure mechanics show that the aluminium  
 341 starts to yield at the onset load values. This is considered to be the failure  
 342 of the specimens for position TC III to TC V. Secondly, the ILSS formula  
 343 shown in section 5.1 is only valid in the linear elastic regime. The maximum



Position	unit	TC I	TC II	TC III	TC IV	TC V
$\tau_{ILSS}(1-3)$	[N/mm <sup>2</sup> ]	47.6	50.5	23.7	18.3	17.9
$\tau_{ILSS}(4-6)$	[N/mm <sup>2</sup> ]	49.0	50.9	25.0	18.6	18.1

Table 5: Average ILSS for GLARE 5 specimens manufactured by resistance bonding with a mesh stripe.

load of positions TC III to TC V occurs after significant plastic deformation and therefore, the formula is no longer valid.

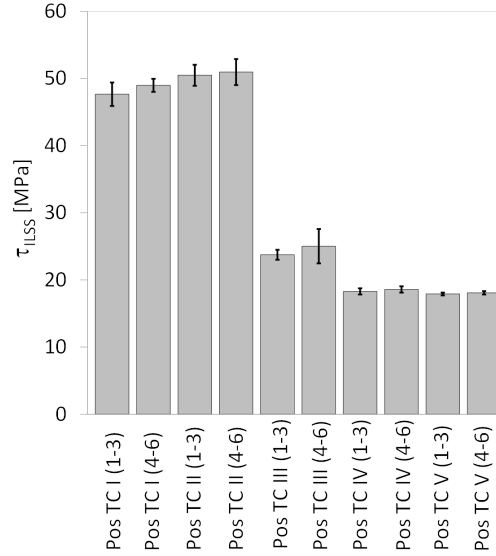


Figure 18: Average ILSS values  $\tau_{ILSS}$  at the positions indicated in Figure 5. The error bars show the scatter range with minimum and maximum ILSS values for each group of specimens.

The average ILSS value of position TC I(1-3), where the mesh stripe was located, was 47.6 MPa. Specimens adjacent to the mesh, TC II (1-3) – 30 mm from the centre of the mesh, had similar ILSS values (50.5 MPa). At distances farther away from the mesh, the average shear strength decreases significantly: at 90 mm distance by 50% (TC III) and from 150 mm on by 60% (TC IV and TC V). ILSS specimens tested in the transverse direction showed similar shear strength values as in the longitudinal direction.

The ILSS values of positions TC I and TC II (47.6 to 50.9 MPa) are of the same order as the one obtained for RB3 specimens (see Table 4, 57.1 MPa).

Both have the same layup. The significant decrease in ILSS values for positions TC III to TC V is related with the different bending behaviour shown by the  $F - \delta$  curve and failure mechanics (significant yield of the aluminium before debonding of the aluminium layers), likely due to low degree of cure.

### 5.2.2. Optical microscopy analysis

In order to assess the mesh impregnation quality and explain the results presented in Section 5.2.1, cross sections were observed by optical microscopy, as was the case for full surface mesh panels. Figure 19 shows cross-sectional images of the panel manufactured by resistance bonding. Locations TC I to TC III, based on Figure 5, are shown from (a) to (d). Good mesh impregnation was observed, even at the transition from TC I to TC II. For location TC III, the presence of large voids in the pure epoxy layers was significant. These voids were also observed at locations further away from the mesh, TC IV to TC V.

These observations can justify and support the significant difference in the mechanical behaviour of the specimens close to the mesh – Positions TC I and TC II, and far from the mesh – Positions TC III, TC IV and TC V. The large voids observed in the latter confirm the poor manufacturing quality and corresponding poor mechanical performance observed at those locations.

## 6. Discussion

### 6.1. Comparison: Autoclave – Resistance bonding – Resistance curing

Based on the ILSS and microscopy results presented in Section 5.1 for the autoclave cured, resistance bonded and resistance cured specimens, three main observations can be highlighted.

Firstly, for the autoclave cured specimens, there were minor to no changes in the quasi-static behaviour and in the cross section quality without (A1, A2, A5 and A6) and with (A3, A4, A7 and A8) an embedded stainless steel mesh (see Figures 9 and 11). The most significant difference was noted when comparing the GLARE 3 panels without (A2) and with (A4) an embedded heater mesh when prepreg layers were placed adjacent to the mesh. This was the result of poorer impregnation of the mesh due to lower epoxy volume content (see Figures 12 and 13).

Secondly, the ILSS values, failure modes and corresponding cross section quality were comparable for the autoclave cured and resistance bonded GLARE 3 and GLARE 5 panels. The exception which did not follow this

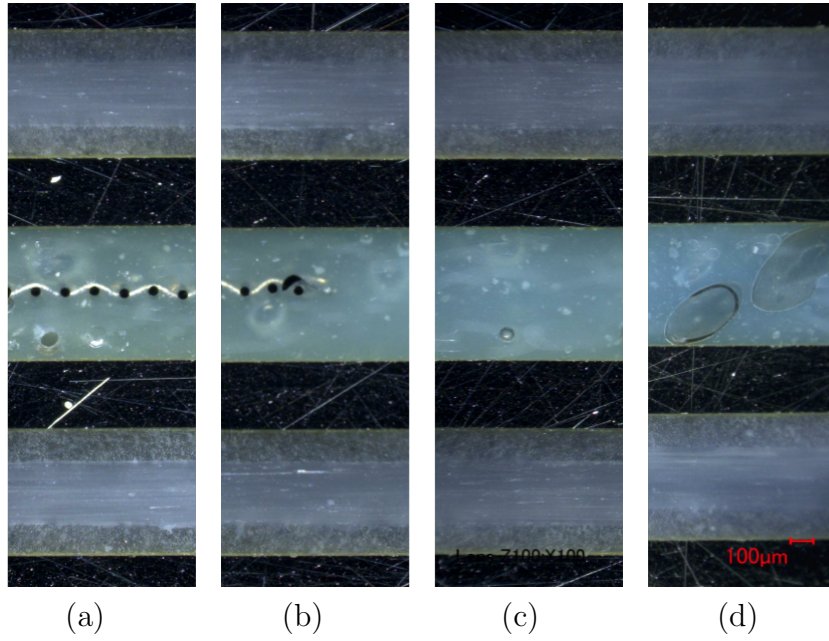


Figure 19: Cross-sectional microscopy images of GLARE 5 panels resistance bonded with a mesh stripe at different locations from the mesh: (a) TC I, (b) Mesh transition between TC I and TC II, (c) TC II, and (d) TC III. Scale: 100  $\mu\text{m}$ .

trend was, similarly to the autoclave cured panels, the resistance bonded GLARE 3 panel with prepreg layers adjacent to the mesh (RB2 panel). It is assumed that the epoxy volume content was not sufficient to impregnate the heater mesh properly. Therefore, the crack initiated at the epoxy-heater mesh interface for RB2 specimens (Figure 10 (c)).

Finally, the resistance curing method produced panels of distinctively lower quality with an increased presence of voids in all prepreg layers (including the ones adjacent to the heater mesh). This led to a decrease in the ILSS values and the onset of failure in the outer prepreg layers. As voids disrupt the homogeneity of the material and act as crack initiators, a higher void content consequently increases the chance of failure at lower stress values and thus, leads to a decrease of the (static) strength. However, this behaviour was more noticeable for the GLARE 5 specimens, compared to GLARE 3, as the void content was likely higher with a lower aluminium surface area over the cross-section (see Section 2).

## 6.2. Degree of cure vs ILSS – Resistance bonding with mesh stripe

Using a mesh stripe instead of a full surface mesh for resistance bonding of GLARE panels severely affects the temperature distribution (see Figure 7). Thus, the aim of this study was to monitor the in-plane temperature distribution during resistance bonding to investigate its effect on the degree of cure and ILSS values at different positions from the mesh (Figure 5).

As previously presented in Figure 18, reasonable ILSS values were determined at locations TC I and TC II, corresponding to distances of up to 30 mm from the heater mesh. Knowing the temperature profiles at different positions (Figure 7), the degree of cure,  $\alpha$ , can be estimated from TC I to TC V based on Kamal-Sourour’s cure kinetics model presented in [39]. In order to do so, three main assumptions were made. Firstly, the same heating/cooling rate for all positions as the one used in the standard manufacturing cycle was assumed ( $\pm 2^\circ\text{C}$ ). Secondly, the maximum temperature at each position remained constant for 60 min. Finally, these constant temperature values for TC I to TC V were assumed to be equal to  $130^\circ\text{C}$ ,  $120^\circ\text{C}$ ,  $80^\circ\text{C}$ ,  $60^\circ\text{C}$  and  $50^\circ\text{C}$ . The expected degree of cure is plotted in Figure 20, along with the corresponding average ILSS values,  $\tau_{ILSS}$ , as shown in Section 5.2.1.

For both cases, as the distance from the mesh increases, the degree of cure and ILSS values significantly drop between 30 mm (TC II) and 90 mm (TC III), which is consistent with literature on epoxy/glass fibre systems submitted to different cure cycles [40]. These findings suggest that

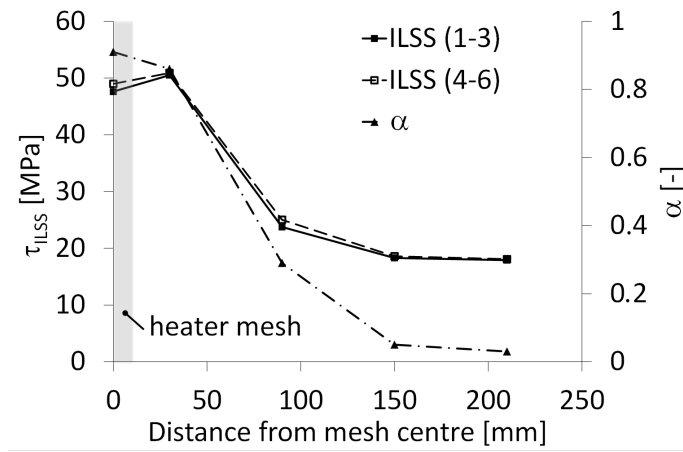


Figure 20: Average ILSS values ( $\tau_{ILSS}$ ) and estimated degree of cure,  $\alpha$ , at different positions from the heater mesh stripe (based on Figure 5).

427 using a spacing of approximately 60 mm between mesh stripes would allow  
 428 to maintain reasonable degree of cure and manufacturing quality. This can  
 429 provide flexibility in the case where a more complex mesh geometry might  
 430 be required depending on the parts to be resistance bonded.

## 431 7. Conclusions

432 Three manufacturing techniques for GLARE panels were investigated and  
 433 compared: full autoclave curing, resistance bonding of two autoclave-cured  
 434 panels, and complete out-of-autoclave resistance curing. For the latter two  
 435 methods, a steel mesh was placed at the panels' mid-plane for bonding or  
 436 curing through resistance heating. The effect of the heater element was  
 437 investigated as a first step for autoclave cured panels. No major differences  
 438 in the static behaviour and manufacturing quality were found between panels  
 439 with and without an embedded heater mesh.

440 The comparison of the different manufacturing techniques and layups  
 441 with an embedded steel mesh across the whole surface at the mid-plane  
 442 showed that resistance bonding is a promising technique which leads to com-  
 443 parable ILSS values to the fully autoclave cured samples with a maximum  
 444 decrease of 10%. Resistance cured samples however **do not show sufficient**  
 445 **manufacturing quality. The significant presence of voids leads to a decrease**  
 446 **of the ILSS values**, especially for the GLARE 5 samples. In all cases, the

importance of a proper mesh impregnation was noted. The best quality was obtained with pure epoxy layers at the mesh interface, while the use of only one prepreg layer on each side of the mesh was more likely to promote crack initiation.

As a first step toward a flexible heater mesh geometry, two GLARE 5 panels were resistance bonded using a 12.5 mm wide (stripe) heater element. The study showed that the degree of cure and ILSS values at distances larger than 30 mm from the mesh decreased significantly. This suggests that a spacing of 60 mm between mesh stripes would allow to maintain high quality and decrease energy consumption during manufacturing. Further investigation into customisable mesh dimensions for flexible on-site repairs could be a focus of future research.

The promising results obtained for the resistance bonded panels with an embedded mesh across the full surface demonstrated the capability to accomplish comparable quality to autoclave manufacturing with minimal equipment (vacuum bag, power supply and thermocouples). Hence, this flexible technique could eliminate a second costly autoclave cycle in the case where, for instance, doublers or stringers need to be bonded to GLARE panels. Furthermore, it can be used for assembly of larger GLARE panels through e.g. resistance bonded scarf joints.

## Acknowledgments

This study was partially funded by the Dutch research agency Technology Foundation (STW) and by Fokker Aerostructures.

## References

- [1] Vogelesang LB, Vlot A. Development of fibre metal laminates for advanced aerospace structures. *Journal of Materials Processing Technology* 2000;103:1 – 5.
- [2] Pettit R. Fiber/metal laminate. Patent US 5227216 A; USPTO.; 1993.
- [3] Vlot A, Gunnink JW. In: Vlot A, Gunnink JW, editors. *Fibre metal laminates – an introduction*. Dordrecht, The Netherlands: Kluwer Academic Publishers; 2001,.
- [4] Vlot A. *Glare – history of the development of a new aircraft material*. Dordrecht, The Netherlands: Kluwer Academic Publishers; 2001.

- 480 [5] Alderliesten RC, Homan JJ. Fatigue and damage tolerance issues of  
481 Glare in aircraft structures. *International Journal of Fatigue* 2006;28  
482 (10):1116 – 1123.
- 483 [6] Hinz S, Omoori T, Hojo M, Schulte K. Damage characterisation of fibre  
484 metal laminates under interlaminar shear load. *Composites: Part A*  
485 2009;40:925 – 931.
- 486 [7] Sadighi M, Pärnänen T, Alderliesten R, Sayeafabi M, Benedictus R.  
487 Experimental and numerical investigation of metal type and thickness  
488 effects on the impact resistance of fiber metal laminates. *Applied Com-  
489 posite Materials* 2012;19 (3):545 – 559.
- 490 [8] Park SY, Choi WJ, Choi HS. The effects of void contents on the long-  
491 term hygrothermal behaviors of glass/epoxy and GLARE laminates.  
492 *Composite Structures* 2010;92 (1):18 – 24.
- 493 [9] Vlot A. Impact loading on fibre metal laminates. *International Journal  
494 of Impact Engineering* 1996;18:291 – 307.
- 495 [10] Centea T, Grunenefelder LK, Nutt SR. A review of out-of-autoclave  
496 prepregs - Material properties, process phenomena, and manufacturing  
497 considerations. *Composites Part A: Applied Science and Manufacturing*  
498 2015;70:132 – 154.
- 499 [11] Tong R, Hoa S, Chen M. Cost analysis on l-shape composite component  
500 manufacturing. *Proceedings of the 18th International Conference on  
501 Composites Materials* 2011;.
- 502 [12] Bader M. Selection of composite materials and manufacturing routes for  
503 cost-effective performance. *Composites: Part A* 2002;33 (7):913 – 934.
- 504 [13] Sinke J. Manufacturing of GLARE Parts and Structures. *Applied Com-  
505 posite Materials* 2003;10:293 – 305.
- 506 [14] Slagter WJ. On the Bearing Strength of Fibre Metal Laminates. *Journal  
507 of Composite Materials* 1992;26 (17):2542 – 2566.
- 508 [15] van Rooijen RGJ, Sinke J, de Vries TJ, van der Zwaag S. The Bearing  
509 Strength of Fibre Metal Laminates. *Journal of Composite Materials*  
510 2006;40 (1):5 – 19.

- 511 [16] Hagenbeek M. Characterisation of Fibre Metal Laminates under  
512 Thermo-mechanical Loadings. PhD thesis; TU Delft; 2005.
- 513 [17] Hinz S, Heidemann J, Schulte K. Damage evaluation of glare4b under  
514 interlaminar shear loading at different temperature conditions. *Adv*  
515 *Compos Lett* 2005;14(2):47 – 55.
- 516 [18] Costa AA, da Silva DFNR, Travessa DN, Botelho EC. The effect of  
517 thermal cycles on the mechanical properties of fibermetal laminates.  
518 *Materials and Design* 2012;42 (1):434 – 440.
- 519 [19] Müller B, Teixeira De Freitas S, Sinke J. Thermal cycling fiber metal  
520 laminates: Considerations, test setup and results. *Proc of the ICCM:*  
521 *20th Int Con on Composite Materials* 2015;;1 – 11.
- 522 [20] Müller B, Hagenbeek M, Sinke J. Thermal cycling of (heated) fibre  
523 metal laminates. *Composite Structures* 2016;152:106 –16.
- 524 [21] Glauser T, Johansson M, Hult A. A comparison of radiation and thermal  
525 curing of thick composites. *Macromol Mater Eng* 2000;274:25 – 30.
- 526 [22] Nightingale C, Day RJ. Flexural and interlaminar shear strength prop-  
527 erties of carbon fibre/epoxy composites cured thermally and with mi-  
528 crowave radiation. *Composites Part A* 2002;33:1021 – 1030.
- 529 [23] Tanrattanakul V, Jaroendee D. Comparison Between Microwave and  
530 Thermal Curing of Glass Fiber-Epoxy Composites: Effect of Microwave-  
531 Heating Cycle on Mechanical Properties. *Journal of Applied Polymer*  
532 *Science* 2006;102:1059 – 1070.
- 533 [24] Joseph C, Viney C. Electrical resistance curing of carbon-fibre/epoxy  
534 composites. *Composites Science and Technology* 2000;60:315 – 319.
- 535 [25] Mahdi S, Kim HJ, Gama BA, Yarlagadda S, Gillerspie Jr. JW. A Com-  
536 parison of Oven-cured and Induction-cured Adhesively Bonded Com-  
537 posite Joints. *Journal of composite materials* 2003;37 (6):519 – 542.
- 538 [26] C. Severijns S. Teixeira de Freitas JP. Susceptor-assisted induction cur-  
539 ing behaviour of a two component epoxy paste adhesive for aerospace ap-  
540 plications. *International Journal of Adhesion and Adhesives* 2017;75:155  
541 – 164.



- 542 [27] Ageorges C, Ye L. Resistance welding of thermosetting compos-  
543 ite/thermoplastic composite joints. *Composites part A* 2001;32:1603  
544 – 1612.
- 545 [28] Yousefpour A, Hojjati M, Immarigeon JP. Fusion bonding/welding of  
546 thermoplastic composites. *Journal of Thermoplastic Composite Materi-*  
547 *als* 2004;17(4):303 – 341.
- 548 [29] Dube M, Hubert P, Yousefpour A, Denault J. Resistance welding of  
549 thermoplastic composites skin/stringer joints. *Composites Part A: Ap-*  
550 *plied Science and Manufacturing* 2007;38 (12):2541 – 2552.
- 551 [30] Shi H. Resistance welding of thermoplastic composites – Process and  
552 performance. PhD thesis; TU Delft; 2014.
- 553 [31] Villegas I, Bersee HEN. Characterisation of a metal mesh heating el-  
554 element for closed-loop resistance welding of thermoplastic composites.  
555 *Journal of Thermoplastic Composite Materials* 2015;28:46 – 65.
- 556 [32] Rider AN, Wang CH, Cao J. Internal resistance heating for homogeneous  
557 curing of adhesively bonded repairs. *International Journal of Adhesion*  
558 *& Adhesives* 2011;31:168 – 176.
- 559 [33] Ashrafi M, Santosh D, Tuttle ME. Resistive embedded heating for ho-  
560 mogeneous curing of adhesively bonded joints. *International Journal of*  
561 *Adhesion & Adhesives* 2015;57:34 – 39.
- 562 [34] Smith B, Ashrafi M, Tuttle M, Devasia S. Bondline Temperature Control  
563 for Joining Composites with an Embedded Heater. *Journal of Manufac-*  
564 *turing Science and Engineering* 2016;138 (2):1087 – 1357.
- 565 [35] Ramakrishnan B, Zhu L, Pitchumani R. Curing of Composites Using  
566 Internal Resistive Heating. *Transactions of the ASME* 2000;122:124 –  
567 131.
- 568 [36] Zhu L, Pitchumani R. Analysis of a process for curing composites by  
569 the use of embedded resistive heating elements. *Composites Science and*  
570 *Technology* 2000;60:2699 – 2712.
- 571 [37] Bwire . <http://wirecloth.bwire.com>, accessed 3.7.2015. 2015;.

- 572 [38] ASTM . Standard Test Method for Short-Beam Strength of Polymer  
573 Matrix Composite Materials and Their Laminates. ASTM standard  
574 D2344/D2344M-13; ASTM International.; 2013.
- 575 [39] Abouhamzeh M, Sinke J, Jansen K, Benedictus R. Kinetic and thermo-  
576 viscoelastic characterisation of the epoxy adhesive in glare. Composite  
577 Structures 2015;124:19 – 28.
- 578 [40] Hong X, Hua Y. The effects of curing cycles on properties of the epoxy  
579 system 3221/RH glass fabric composites. Polymer Composites 2008;29  
580 (4):364 – 371.